

---

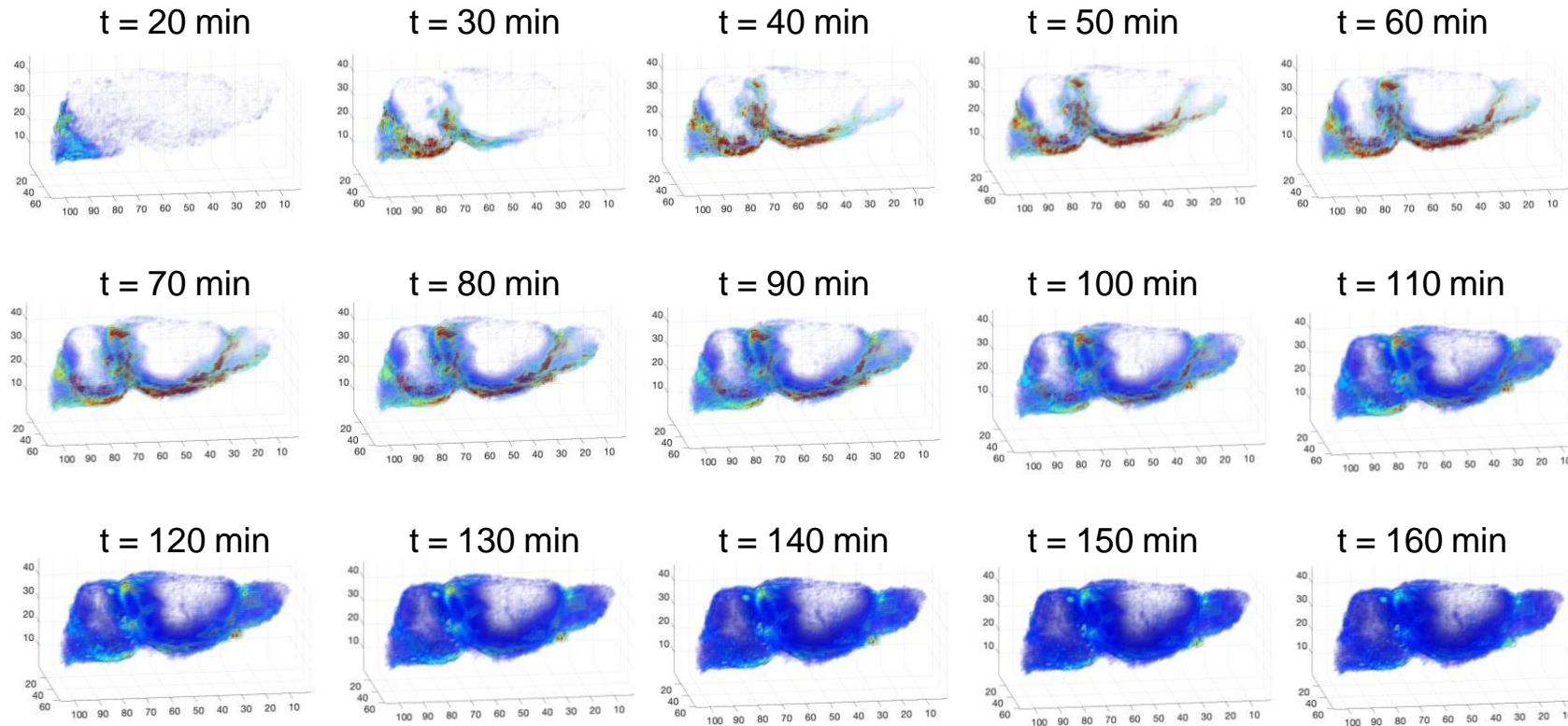
**Supplementary information**

---

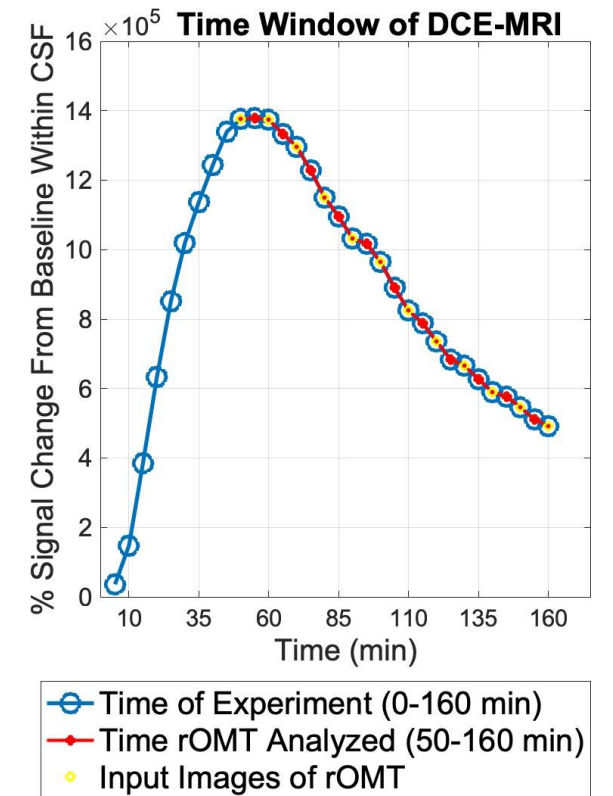
**Cerebral amyloid angiopathy is associated with glymphatic transport reduction and time-delayed solute drainage along the neck arteries**

---

In the format provided by the authors and unedited

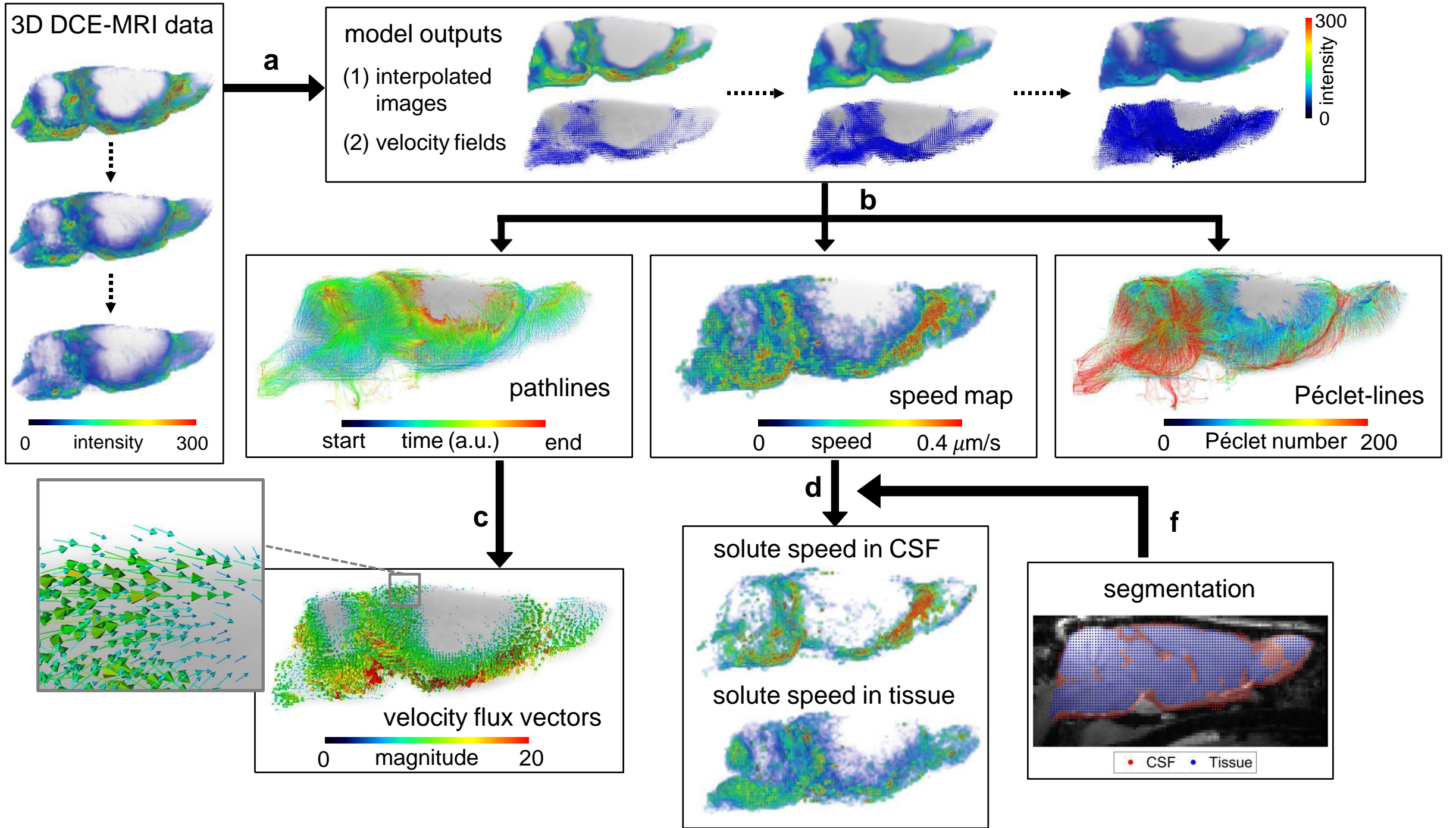
**a**

0      intensity (% signal change from baseline)      300

**b**

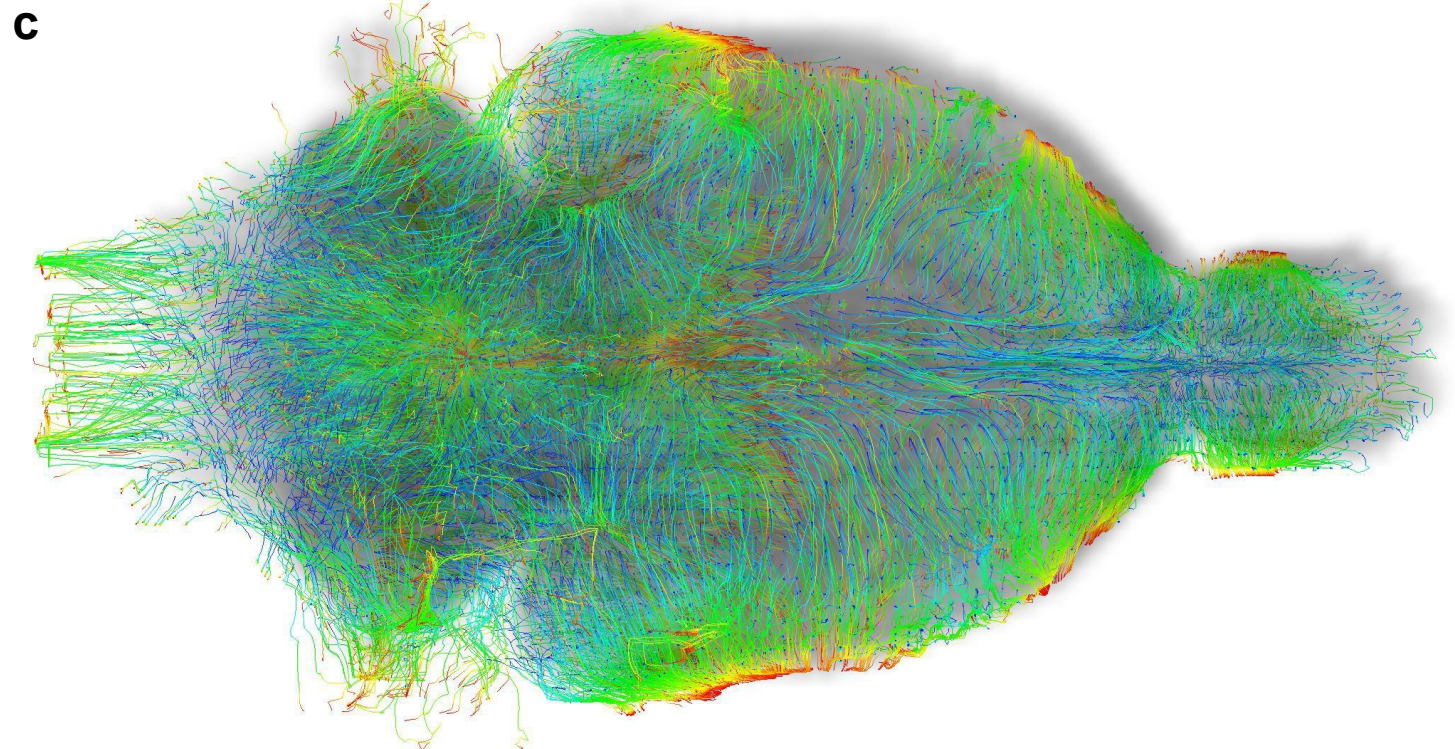
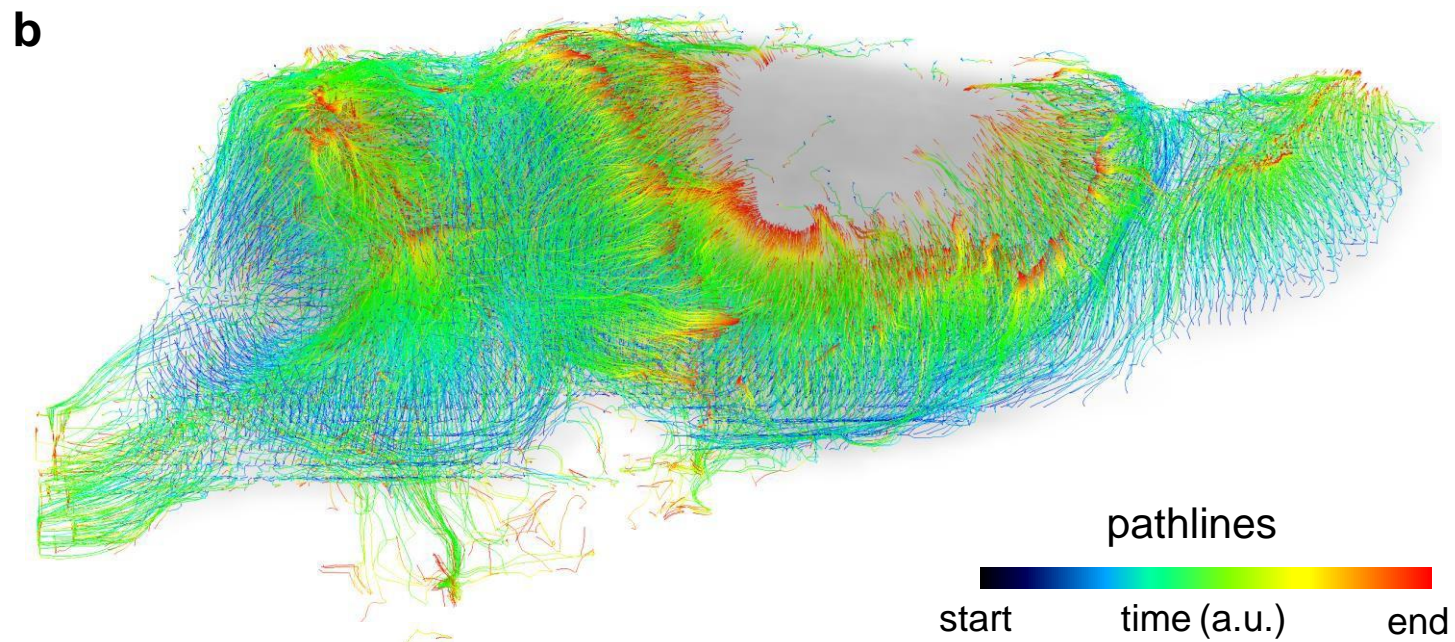
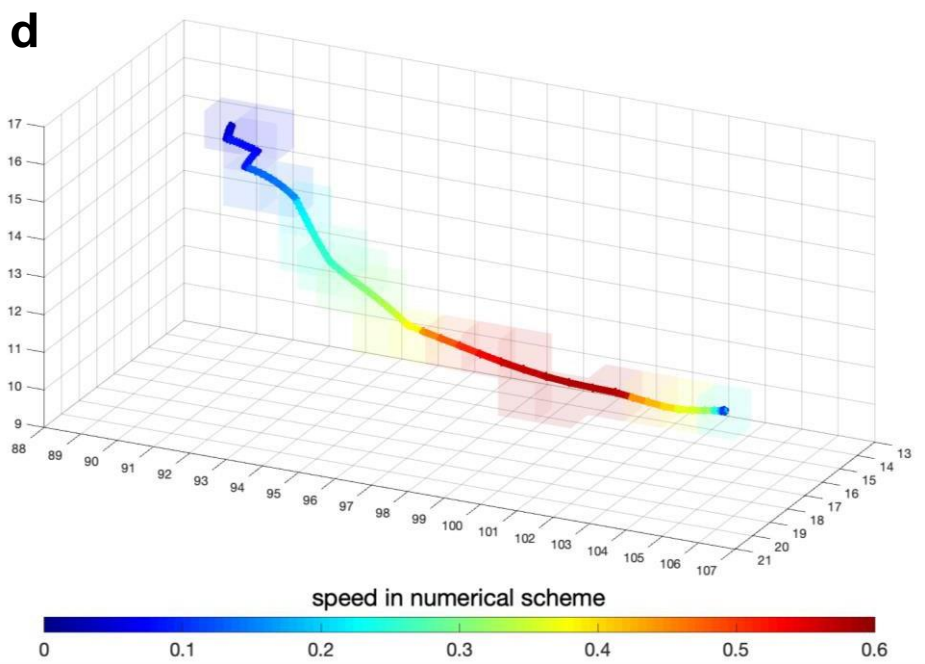
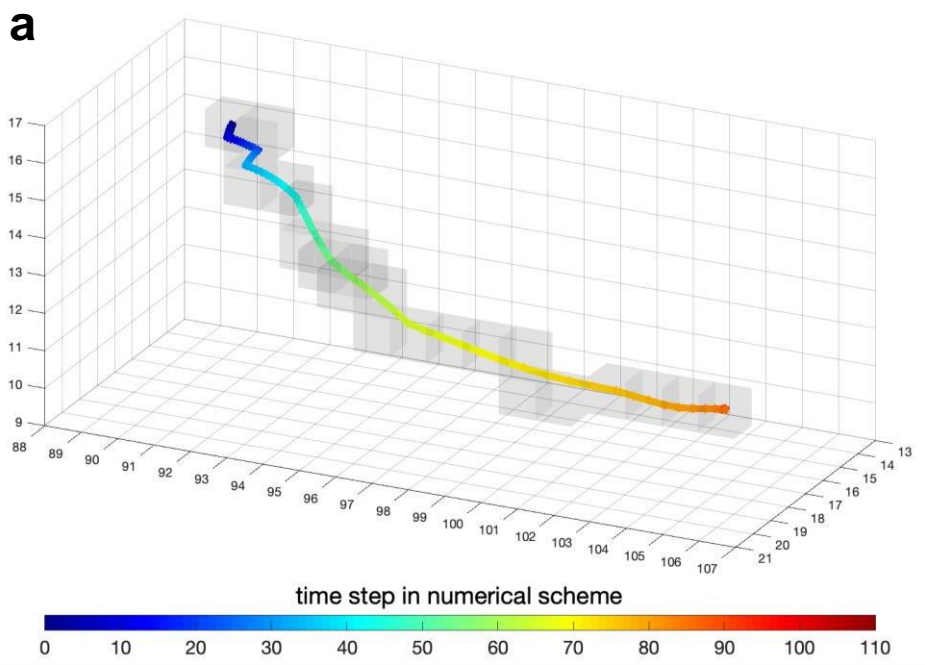
**Supplementary Information Fig. 1: Data processed with the regularized optimal mass transport (rOMT) algorithm**

**a** In our experiments, we injected tracers into the cerebrospinal fluid (CSF) of rat brains via the cisterna magna and scanned the brains with MRI every 5 minutes over ~2 hours. The acquired MRI data was further processed based on the % signal change from baseline to obtain the dynamic contrast enhanced MRI (DCE-MRI) data of 55 rats. Here we show the DCE-MRI data of an example 12-month-old wild type rat brain at different time frames. **b** We analyzed the DCE-MRI data between the 50-minute (min) and 160-min with the rOMT algorithm. By starting approximately 1~3 frames before the total signal peak in the CSF compartment, we ensure that the tracers have almost fully entered the CSF of rat brains. We put every other image in this time period into the rOMT model for the purpose of saving running time. This figure shows the total DCE-MRI intensity in the CSF of the example rat over time.



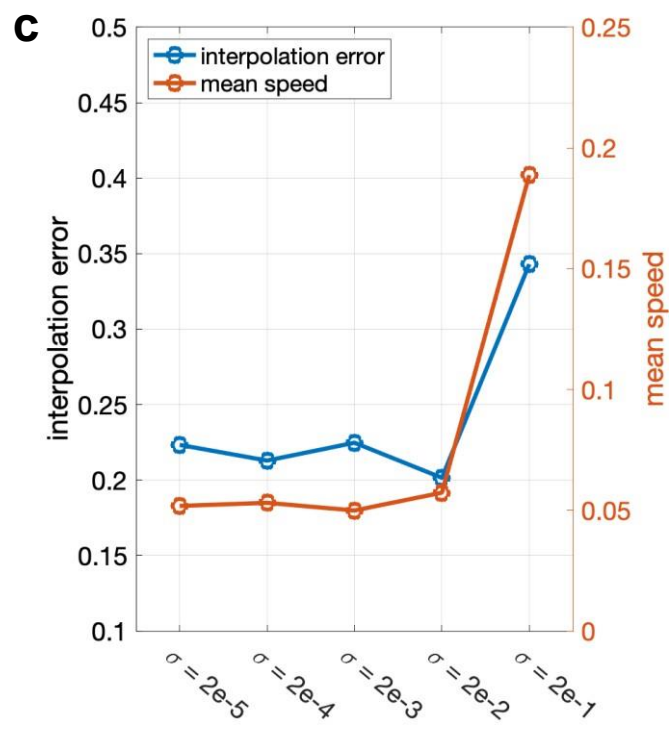
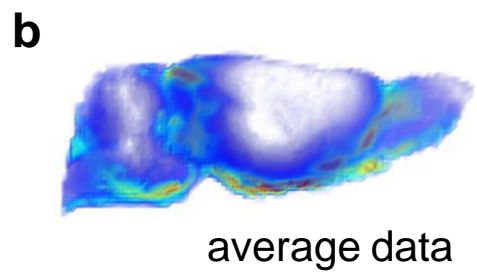
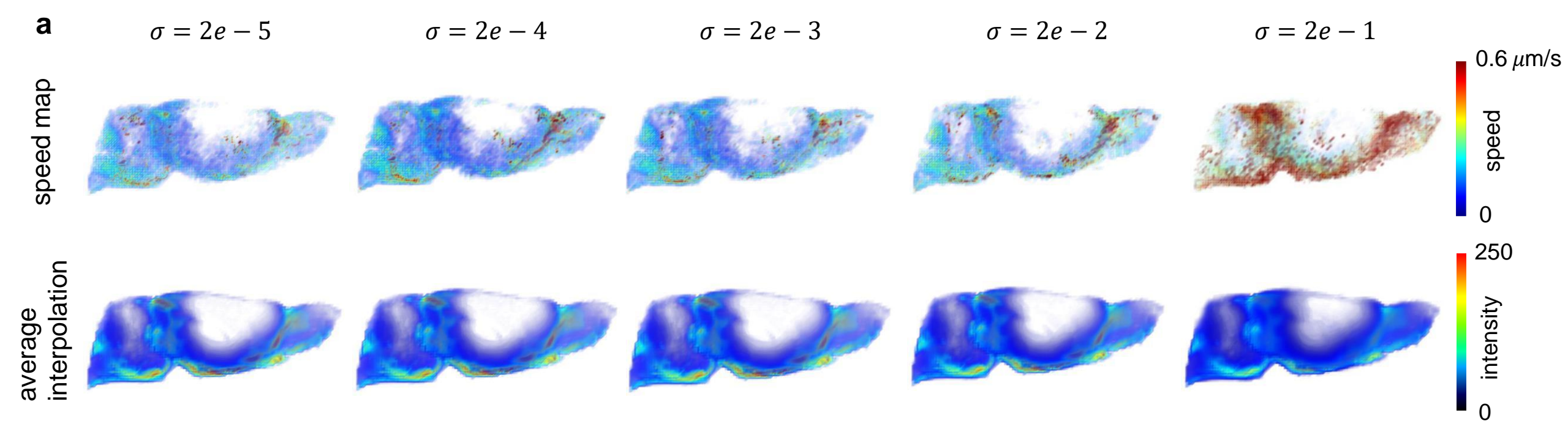
**Supplementary Information Fig. 2: Pipeline of regularized optimal mass transport (rOMT) data analysis**

**a** We feed the dynamic contrast enhanced MRI (DCE-MRI) data of rat brains into the rOMT algorithm. **b** Interpolated images and velocity fields, which are returned from the rOMT computational process, are used to derive binary pathlines (trajectories of solute movement), speed maps and Péclet-lines under the proposed Lagrangian representation of the Glymphatic Dynamics framework. The color code of the pathlines provides a spatial visualization of the starting and end points of each pathline. The speed map reflects the activity intensity distribution within the rat brain with red and blue representing relatively fast and slow solute speed, respectively. The Péclet-lines, which consist of local Péclet numbers along pathlines, indicate advection-dominated regions with higher Péclet values and diffusion-dominated regions with lower values. **c** Velocity flux vectors, which are color coded by the magnitude of vectors, are computed by connecting the initial and end points of pathlines. These vectors provide the directional information of the dynamic stream whose magnitude indicates the distance for how far a given particle has transported over a finite time frame. **d-f** CSF and tissue (glymphatic) segmentation of the brain separates the given speed map into corresponding sub-maps. Two measurements, *speed* and *v-flux*, are calculated to measure the mean speed and the total volume of transport involved in the CSF and tissue compartments, respectively.



### Supplementary Information Fig. 3: Details of the Lagrangian representation of Glymphatic Dynamics (GLaD) Method

**a** From the returned outputs of the regularized optimal mass transport (rOMT) algorithm, we are able to compute and plot the discrete binary pathlines of solutes following the Lagrangian coordinates. In this figure, one example pathline is shown color coded by the order of numerical steps. The number of numerical cells through which this pathline passes (the grey boxes) is called the *volume flux* (*v-flux*) associated with this pathline. **b, c** Superimposing all the pathlines on the anatomical background of the rat brain, we show that the GLaD method is capable of tracing solute pathways under the fluid dynamics within the brain. The volume flux of all the pathlines reflects the size of the glymphatic system involved in the fluid dynamic. **d** If we endow the binary pathlines with the speed or Péclet number and interpolate these values into the nearest numerical cell center, we will derive the corresponding speed map or *Pe* map. This figure illustrates how one pathline endowed with speed is interpolated into data resolution (also the size of numerical grid) which are the boxes color coded by the intensity of speed.





#### Supplementary Information Fig. 4: Choice of Diffusivity of regularized optimal mass transport (rOMT)

**a, b** The diffusivity in our work is a positive constant denoted as  $\sigma$ . We tested our rOMT algorithm with  $\sigma = 2e - 5$ ,  $\sigma = 2e - 4$ ,  $\sigma = 2e - 3$ ,  $\sigma = 2e - 2$  and  $\sigma = 2e - 1$  on a sample 12-month-old wild type rat dataset. Two important outputs, the speed map and average interpolation, as well as the average data are shown in the figure for comparative visualization. **c** We computed the mean speed and the interpolation error of all five diffusivity values intended for a quantitative comparison. The mean speed is derived from the mean of all non-zero values in the speed map. The interpolation error reflects the closeness of returned interpolations from rOMT and the data put into rOMT. The lower the interpolation error is, the more accurate the rOMT algorithm is matching the real data. The speed map shows a stable trend in the range between  $\sigma = 2e - 5$  and  $\sigma = 2e - 3$ . When  $\sigma$  gets even higher, the speed becomes higher overall and “explodes” when  $\sigma = 2e - 1$ . When  $\sigma = 2e - 5$ ,  $\sigma = 2e - 4$ ,  $\sigma = 2e - 3$  and  $\sigma = 2e - 2$ , the interpolations match the data well with the interpolation error remains at a low level. However, the image gets way too smooth when  $\sigma$  goes to  $2e - 1$  probably because the diffusion is playing too much a role, and the corresponding interpolation error also “explodes”. By considering both the accuracy of rOMT matching the data and the stability on the speed information, we believe  $\sigma = 2e - 3$  is a safe choice.